Alpha-synuclein enhances lipid droplet accumulation in neurons in a *Drosophila* model of Parkinson's disease

Victor Girard[1], Florence Jollivet[1], Oskar Knittelfelder[2], Jean-Noel Arsac[3], Gilles Chatelain[1], Daan M. Van den Brink[1,4], Thierry Baron[3], Andrej Shevchenko[2], Nathalie Davoust-Nataf[1,*], Bertrand Mollereau[1,*]

[1] Laboratory of Biology and Modelling of the Cell, UMR5239 CNRS/ENS de Lyon, INSERM U1210, UMS 3444 Biosciences Lyon Gerland, University of Lyon, F-69342, Lyon, France.
[2] Max-Planck-Institute of Molecular Cell Biology and Genetics, Pfotenhauerstraße 108, 01307 Dresden, Germany.
[3] Neurodegenerative Disease Unit; French Agency for Food, Environmental and Occupational Health & Safety (Anses) Laboratory of Lyon, Université de Lyon, Lyon, France.
[4] Plant Systems Physiology, Institute for Water and Wetland Research, Radboud University, PO Box 9010, 6500 GL Nijmegen, The Netherlands.

*Co-senior and co-corresponding authors: nathalie.davoust-nataf@ens-lyon.fr and bertrand.mollereau@ens-lyon.fr

Abstract

Parkinson's disease is a neurodegenerative disorder characterized by accumulation of alpha-synuclein (αSyn) aggregates and by abnormalities in lipid storage. To investigate the potential pathophysiological consequences of interactions between αSyn and proteins that regulate the homeostasis of intracellular lipid droplets (LDs), we employed a transgenic *Drosophila* model of PD in which human αSyn is specifically expressed in photoreceptor neurons. We found that overexpression of the LD-coating proteins perilipin 1 and 2 (dPlin1/2) markedly increased LD accumulation in the neurons. Perilipins also co-localized with αSyn at the LD surface in both *Drosophila* photoreceptor neurons (dPlin2) and human neuroblastoma cells (PLIN3). Co-expression of αSyn and dPlin2 in photoreceptor neurons synergistically amplified LD content through a mechanism involving LD stabilization, independently of *Brummer*-mediated lipolysis or *de novo* synthesis of triacylglycerols. Accumulation of LDs also increased the resistance of αSyn to proteolytic digestion, a phenomenon associated with αSyn aggregation in human neurons. Our results suggest that binding of αSyn to PLIN-coated LDs stabilizes the LD structure and may contribute to the pathogenic misfolding and aggregation of αSyn in neurons.

Introduction

Lipids play crucial roles in many essential cellular functions, including membrane formation, energy production, intracellular and intercellular signal transduction, and regulation of cell death. Fatty acids (FAs) taken up into or synthesized within cells are stored in discrete organelles known as lipid droplets (LDs), which consist of a core of neutral lipids (predominantly triacylglycerols [TGs] and sterol esters), surrounded by a monolayer of phospholipids containing numerous peridroplet proteins (Olzmann and Carvalho, 2019). Maintenance of LD homeostasis in adipose tissue and the central nervous system, among other tissues, has emerged as a central process for organismal health, and its dysregulation contributes to many human diseases, such as obesity, atherosclerosis, fatty liver disease, and neurodegenerative disorders such as Parkinson's disease (PD) (Fanning et al., 2020; Farmer et al., 2020; Krahmer et al., 2013; Pennetta and Welte, 2018).

Several peridroplet proteins regulate the homeostasis and abundance of LDs by controlling their biogenesis, degradation, and/or structural stabilization (Olzmann and Carvalho, 2019). LD biogenesis is initiated at the endoplasmic reticulum membrane, where key lipid metabolic enzymes such as diacylglycerol acyltransferase 1 and 2 (DGAT1, DGAT2) and FA transport protein 1 (FATP1) are recruited. These enzymes synthesize TGs that are incorporated into the LD (Dourlen et al., 2015; Thiam and Beller, 2017; Walther et al., 2017). LD degradation is mediated by lipases such as adipose triglyceride lipase (ATGL) and hormone-sensitive lipase (Zechner et al., 2012). In turn, lipase activity is controlled by a family of peridroplet proteins called perilipins (PLINs) that play different roles in LD homeostasis, including maintaining LD integrity, limiting basal lipolysis, and interacting with mitochondria (Kimmel and Sztalryd, 2016). The human genome encodes five PLIN proteins, PLIN1–5 (Kimmel and Sztalryd, 2016), whereas the *Drosophila* genome encodes two PLINs, Lsd-1 and Lsd-2 (hereafter named dPlin1 and dPlin2) (Heier and Kühnlein, 2018), that have redundant functions in controlling lipolysis (Beller et al., 2010; Bi et al., 2012). *dPlin1* expression, like that of human *PLIN1*, is restricted to adipose tissue, while *dPlin2* and human *PLIN2* and *3* are expressed ubiquitously (Itabe et al., 2017). Although LDs are present in all cells, relatively few types are particularly prone to LD accumulation (Beller et al., 2020). These include adipocytes and glial cells, which have a higher rate of FA synthesis and express tissue-specific peridroplet proteins that promote the biogenesis or stabilization of LDs or

inhibit their lipolytic degradation. About 200 peridroplet proteins have been identified to date (Bersuker and Olzmann, 2017; Bersuker et al., 2018; Olzmann and Carvalho, 2019), but their cellular specificity and precise involvement in the regulation of LD biogenesis, stabilization, and degradation are largely unknown.

The mechanisms by which fat is stored and remobilized in LDs in adipose tissue are relatively well understood (Heier and Kühnlein, 2018); in contrast, less is known about the non-lipid storage functions of LDs, such as their involvement in the regulation of cellular stress and protein handling, folding, and turnover (Olzmann and Carvalho, 2019; Welte and Gould, 2017). This situation has improved in the last few years; for example, studies with *Drosophila* and vertebrate cellular models have begun to unravel the pathophysiological roles of LDs in regulating stress in cells of the nervous system. Oxidative stress exposure or excitotoxicity induces LD accumulation in developing or adult *Drosophila* and in mouse glial cells co-cultured with neurons (Bailey et al., 2015; Ioannou et al., 2019; Liu et al., 2015, 2017; Van Den Brink et al., 2018). In *Drosophila* larvae subjected to hypoxia, LD accumulation in glial cells is thought to play a neuroprotective role by enabling relocation of lipids sensitive to peroxidation, such as polyunsaturated FAs, from membrane phospholipids to TGs in the LD core (Bailey et al., 2015). While LDs are abundant in glial cells, they are rarely detected in neurons and little is known about their potential pathophysiological relevance to neurological diseases (Welte, 2015).

PD is characterized by the neuronal accumulation of misfolded proteins, including α-synuclein (αSyn), in cytoplasmic aggregates known as Lewy bodies (Poewe et al., 2017; Shahmoradian et al., 2019). αSyn is a vertebrate-specific 14-kDa presynaptic protein and contains an N-terminal domain consisting of repeated sequences of 11 amino acids that fold into an amphipathic helix upon lipid binding (Bussell and Eliezer, 2003). Although the physiological function of αSyn is still unclear, several lines of evidence indicate that αSyn binding to phospholipid membranes is important for vesicle dynamics at the synapse (Auluck et al., 2010). Importantly, αSyn has been shown to bind to LDs and to contribute to LD homeostasis by regulating TG synthesis and lipolysis, although the exact underlying molecular mechanisms are unknown (Cole et al., 2002; Čopič et al., 2018; Fanning et al., 2019; Outeiro and Lindquist, 2003; Sánchez Campos et al., 2018; Thiam et al., 2013). Biophysical and biochemical studies have demonstrated that the aberrant association of

αSyn with lipid membranes affects αSyn oligomerization and aggregation (Galvagnion, 2017; Suzuki et al., 2018). Collectively, these findings have suggested that αSyn–LD interactions may be involved in synucleinopathies such as PD.

Here, we tested this hypothesis *in vivo* using a *Drosophila* model of PD in which human αSyn is expressed specifically in photoreceptor neurons. This transgenic model exhibits little to no neuronal toxicity and it has proven useful in studies of αSyn conversion to a proteinase K-resistant form prone to aggregation, as is seen in human PD (Auluck et al., 2002; Feany and Bender, 2000; Suzuki et al., 2015). We investigated the effects of PLIN and αSyn expression on LD formation in neurons; the subcellular co-localization of αSyn with LDs; the potential contribution of αSyn/PLINs to LD homeostasis via regulation of LD formation, stabilization, and/or degradation; and the potential effects of αSyn–LD binding on the susceptibility of αSyn to misfolding in the context of PD.

Results

αSyn synergizes with PLIN proteins to induce LD accumulation in neurons

Several studies have reported that expression of human αSyn dysregulates TG metabolism and LD homeostasis in cellular and rodent models of PD (Cole et al., 2002; Fanning et al., 2019; Han et al., 2018; Outeiro and Lindquist, 2003; Sánchez Campos et al., 2018). As noted above, LD homeostasis crucially relies on peridroplet proteins. To determine whether the function of PLINs in LD homeostasis is influenced by αSyn expression, we first established the dynamics of LD homeostasis in *Drosophila* neurons. The *Drosophila* compound eye is composed of 800 ommatidia, each containing six outer and two inner photoreceptor neurons surrounded by nine retina pigment/glial cells (Figure S1) (Mollereau and Domingos, 2005). *dPlin1::GFP* (Beller et al., 2010) and *dPlin2::GFP* (Grönke et al., 2003) were expressed specifically in outer photoreceptor neurons of flies using a rhodopsin 1 (*Rh1*) driver, and the abundance of LDs was assessed by co-labeling of whole-mount retinas with the lipophilic fluorophore Bodipy to label LDs. This analysis revealed that, while LDs were virtually undetectable in the retina of 20-day-old control flies, *dPlin1::GFP* or *dPlin2::GFP* overexpression led to accumulation of LDs (measured as the percentage of the retina area stained with Bodipy, Figure 1A, B). Next, we determined whether this effect of dPlin expression was specific to neurons or also observed in surrounding glial cells, we immunostained the retina for the Na^+/K^+ ATPase α subunit, a marker of the photoreceptor plasma membrane (Yasuhara et al., 2000). As shown in Figure 1C, *dPlin1::GFP* and *dPlin2::GFP* labeling was visible as rings, characteristic of peridroplet proteins, located within the cytoplasm of photoreceptors but not in the adjacent glial cells. These results indicate that *Rh1*-driven PLIN overexpression leads to accumulation of LDs only in photoreceptor neurons, and not in adjacent glial cells.

Having established that PLIN levels regulate LD accumulation, we next determined whether αSyn co-expression affected LD accumulation in photoreceptor neurons. For this, we employed transgenic *Drosophila* lines expressing wild-type human αSyn^{WT} (Auluck et al., 2002; Chouhan et al., 2016; Cooper et al., 2006; Feany and Bender, 2000; Lessing and Bonini, 2009; Ordonez et al., 2018) together with *dPlin2::GFP*; these flies harbor a relatively low level of LDs, thereby enabling the effects of αSyn to be detected (Figure 1D). Notably, while photoreceptor neuron-specific expression of αSyn^{WT} induced a small but insignificant

increase in LD accumulation compared with control (LacZ) flies, concomitant expression of *αSyn*^{WT} and *dPlin2::GFP* resulted in a striking synergistic effect, more than tripling the abundance of LDs compared with either *αSyn* or *dPlin2::GFP* expression alone (Figure 1D and 1E). This result was confirmed using independent fly lines carrying *UAS-dPlin2::GFP* and *UAS-αSyn*^{WT} transgenes inserted at a different chromosomal localization (Figure S2). Thus, these results indicate that *Drosophila* photoreceptor neurons contain few LDs under normal physiological conditions, and that LD content is significantly increased in a synergistic manner by co-expression of *dPlin2* and *αSyn*.

αSyn and PLINs co-localize at the LD surface in *Drosophila* photoreceptor neurons and in human neuroblastoma cells

Because PLINs are LD membrane-associated proteins, we hypothesized that the synergistic effect of αSyn and PLINs on LD accumulation in neurons might involve co-localization of the proteins at the LD surface. Indeed, immunostaining of αSyn in flies with photoreceptor neuron-specific expression of *dPlin2::GFP* revealed co-localization of the αSyn^{WT} and dPlin2 at the LD surface (Figure 2A). In addition, we examined protein co-localization in the human neuroblastoma cell line SH-SY5Y (Ryu et al., 2002), which expresses *αSyn* at very low levels and was therefore transfected with *αSyn*^{WT}. In these cells, PLIN3 (also known as TIP47), which is broadly expressed in human brain cells (Sjöstedt et al., 2020), co-localized with αSyn^{WT} around circular vesicles, as detected using high-resolution Airyscan microscopy (Figure 2B). To confirm this finding, we performed proximity ligation assays (PLA), in which oligonucleotide-coupled secondary antibodies generate a fluorescent signal when the two target protein-bound primary antibodies are in close proximity (Wang et al., 2015). Confocal microscopy of SH-SY5Y cells co-labeled with Bodipy and primary antibodies against αSyn^{WT} and PLIN3 revealed PLA signals on the surface of LDs (Figure 2C). Taken together, these experiments confirm that αSyn^{WT} co-localizes with the LD-binding protein dPlin2 in *Drosophila* photoreceptor neurons and with PLIN3 in human neuroblastoma cells.

PLINs promote LD accumulation in neurons by stabilizing LDs, and not by modulating LD formation or Brummer-mediated lipolysis

The mechanism(s) by which αSyn and PLINs might cooperate to promote LD accumulation could be mediated through effects on the formation, stabilization, or degradation of LDs. Indeed, PLINs are known to maintain the structure of LDs and protect them from lipolysis (Brasaemle, 2007). We first examined how LDs might be degraded in photoreceptor neurons by RNAi interference-mediated depletion of the main TG lipase *Brummer* (Bmm), the *Drosophila* ATGL ortholog (Grönke et al., 2005) using either a pan-retinal (*GMR-GAL4*) or photoreceptor-specific *(Rh1-GAL4*) driver. Knockdown of *Bmm* using *GMR-GAL4* resulted in LD accumulation between adjacent photoreceptor membranes (Na^+/K^+ ATPase α subunit-positive), indicating that prevention of Bmm-mediated lipolysis increased LD accumulation in glial cells (Figure 3A, B). In striking contrast, photoreceptor-specific knockdown of *Bmm* did not increase LD abundance, indicating that Bmm-mediated lipolysis does not influence LD homeostasis in photoreceptor neurons (Figure 3A). The fact that LD degradation in *Drosophila* photoreceptor neurons does not involve Bmm, the main *Drosophila* lipase, is in contrast with what is observed in other tissues (Grönke et al., 2005). It also suggests that αSyn and dPlin1/2 could not induce LD degradation through a mechanism involving lipolysis.

We next asked whether dPlins can enhance LD accumulation by promoting the activity of two canonical enzymes of TG synthesis; dFatp and midway (Mdy). Mdy is a diacylglycerol acyltransferase that is structurally related to mammalian DGAT1 (Buszczak et al., 2002). For these experiments, we used *dPlin1:GFP* flies because they produce large easily quantified LDs in photoreceptors (Figure 1C). Whereas pan-retinal knockdown of *dFatp* or *Mdy* reduced the accumulation of LDs in glial cells induced by *Bmm* knockdown (Figure S3), photoreceptor neuron-specific knockdown of either *dFatp* or *Mdy* had no effect on LD accumulation in *dPlin1::GFP*-expressing flies (Figure 3C and 3D).These results indicate that PLIN-induced LD accumulation in photoreceptor neurons probably occurs through a mechanism independent of Bmm inhibition or *de novo* TG synthesis, and is thus distinct from the mechanism of LD accumulation in glial cells.

We then considered that PLINs may stabilize the LD structure, as previously proposed in yeast and *Drosophila* fat cells (Beller et al., 2010; Gao et al., 2017). Therefore, we asked

whether additional LD-binding proteins might have effects similar to PLIN overexpression. We examined *Drosophila* expressing a fusion protein of GFP bound to the LD-binding domain (LD^{BD}-GFP) of the protein Klarsicht, that is required for the intracellular transport of LDs in *Drosophila* embryos (Welte et al., 1998; Yu et al., 2011). Additionally, we tested flies overexpressing *CG7900*, the *Drosophila* ortholog of FA amide hydrolase *FAAH2*, which contains a functional LD-binding domain (Kaczocha et al., 2010). Notably, photoreceptor-specific expression of LD^{BD}*-GFP* or *CG7900* (using EP-[UAS] insertion) induced an accumulation of LDs (Figure 3E, 3F, S4) similar to that observed with dPlin overexpression. Taken together, these results show that overexpression of an LD-binding protein is sufficient to promote LD accumulation in *Drosophila* photoreceptor neurons, thus suggesting that PLIN expression induces LD accumulation by stabilizing the LD structure, at least in part.

Co-expression of αSyn^{A53T} and CG7900 proteins induces LD accumulation in *Drosophila* photoreceptor neurons

Given the crucial role of αSyn aggregates in PD and our demonstration of a link between αSyn and LD accumulation in *Drosophila* neurons, we hypothesized that αSyn–LD interactions might have relevance to PD. To test this, we employed the *GMR>*αSyn^{A53T}*-CG7900 Drosophila* line, which expresses a mutant form of αSyn that is not only associated with familial PD but also, like αSyn^{WT}, binds to LDs in HeLa cells and cultured mouse hippocampal neurons (Cole et al., 2002). In the *UAS-*αSyn^{A53T} transgenic line, the insertion occurs in the promoter region of *CG7900* (Figure 4A, chromosomal position 3R-48; see Materials and Methods). GAL4-mediated transcription of *UAS-*αSyn^{A53T} using the *GMR-GAL4* driver resulted in overexpression of both *CG7900* and αSyn^{A53T} (Figure 4A and 4B) and induced the accumulation of LDs, as visualized by Bodipy staining in longitudinal retinal sections (Figure 4C). Electronic microscopy of retina tangential sections of these flies also revealed that LDs accumulated in the cytoplasm of photoreceptors (Figure 4D). Expression of RNAi targeting *CG7900* in the αSyn^{A53T}*-CG7900* transgenic line abolished the accumulation of LDs (Figure S5), indicating that expression of an LD-binding protein was essential to observe the increase in LD accumulation in response to αSyn^{A53T} in photoreceptor neurons, as was also observed for αSyn^{WT}-expressing flies.

Interestingly, lipidomic analyses of retinas revealed that the lipid content of LDs was identical in flies with photoreceptor neuron-specific expression of *αSyn*^{A53T}*-CG7900* and *αSyn*^{WT} with the exception of TGs, which were enriched in *αSyn*^{A53T}*-CG7900* -expressing flies (Figure S6). Consistent with this, Bodipy staining was abolished by overexpressing the TG lipase *Bmm* in *αSyn*^{A53T}*- CG7900* expressing flies (Figure 4E). These results demonstrate that TG is the major lipid in ectopic LD-induced by CG7900.

LDs promote αSyn resistance to proteinase K

In human neurons, αSyn aggregation is a multi-step process involving accumulation of misfolded αSyn, a process that renders αSyn resistant to mild proteolysis using proteinase K (Cremades et al., 2012; Suzuki et al., 2015). Therefore, we determined whether αSyn–LD interactions might influence the physical state/structure of αSyn in *Drosophila* photoreceptor neurons. αSyn resistance to proteinase K was evaluated by western blot analysis of protein extracts from flies overexpressing *αSyn*^{A53T}*-CG7900*, which accumulate LDs as noted above. αSyn^{A53T} from 30-day-old transgenic flies was more resistant to proteinase K digestion compared with αSyn^{A53T} from 6-day-old flies (Figure 5A and 5B), consistent with an age-dependent conversion of αSyn to misfolded forms. Because LDs also accumulate with advancing age, we examined αSyn resistance in *αSyn*^{A53T}*-CG7900* flies depleted of LDs by co-expression of Bmm lipase in photoreceptor neurons. Indeed, depletion of LDs abolished the age-related difference in αSyn^{A53T} resistance to proteinase K digestion (Figure 5A and 5B), providing a direct link between LD abundance and aberrant αSyn folding and/or aggregation. To confirm this link, we performed proteinase K-resistance assays on αSyn^{WT} from 6- and 30-day-old flies in which LD accumulation is increased by *dPlin2* and *αSyn*^{WT} co-expression. We observed that proteinase K-resistance was increased when LD abundance was synergistically increased by expression of both *αSyn*^{WT} and *dPlin2* compared to *αSyn*^{WT} alone in 6-day-old flies (Figure S7A and S7B). This indicates that LD abundance had a crucial influence on αSyn^{WT} proteinase K-resistance. Taken together, these results substantiate our conclusion that LD accumulation enhances the resistance of αSyn to proteinase K.

Discussion

In this study, we investigated the mechanisms that regulate LD homeostasis in neurons, the contribution of αSyn to LD homeostasis, and whether αSyn–LD binding influences the pathogenic potential of αSyn. We found that expression of the perilipins dPlin1 and dPlin2 in *Drosophila* photoreceptor neurons increased LD accumulation and that this was amplified by co-expression of the PD-associated protein αSyn with dPlin2. αSyn co-localized with PLINs on the LD surface in both *Drosophila* photoreceptor neurons and human neuroblastoma cells, as demonstrated by confocal microscopy and PLA assays. PLIN-induced LD accumulation was not dependent on inhibition of ATGL/Bmm or on TG synthesis, suggesting that PLINs act to stabilize existing LDs, rather than to promote their formation or degradation. Finally, we observed that LD accumulation in photoreceptor neurons was associated with an increase in the resistance of αSyn to proteinase K, suggesting that an increase in LDs might promote αSyn misfolding, an important step in the progression to PD. Thus, we have uncovered a potential novel role for LDs and PLINs in the pathogenicity of αSyn in PD.

Our understanding of the mechanisms of LD homeostasis in neurons under physiological or pathological conditions is far from complete. Neurons predominantly synthesize ATP through aerobic metabolism of glucose, rather than through FA β-oxidation, which likely explains the relative scarcity of LDs in neurons compared with glial cells (Schönfeld and Reiser, 2013). Nevertheless, LD accumulation has been observed in cultured primary rat cortical neurons, rat dopaminergic N27 cells expressing αSyn, and SH-SY5Y cells exposed to 1-methyl-4-phenyl-1,2,3,6-tetrahydropyridine, a dopaminergic neurotoxin prodrug that causes PD-like symptoms in animal models (Fanning et al., 2019; Han et al., 2018; Sánchez Campos et al., 2018). Our results indicating that PLIN expression enhances LD content independently of Bmm lipase activity is consistent with previous data showing that neurons from ATGL-mutant mice do not accumulate LDs (Etschmaier et al., 2011). Moreover, our observation that overexpression of Klarsicht lipid-binding domain or CG7900 phenocopied the effect of PLINs on LD accumulation, supports the possibility that PLINs serve to stabilize LDs, rather than promote their degradation or synthesis. Stabilization of LDs could well be an ancestral function of PLINs, as reported for yeast and *Drosophila* adipose tissue (Beller et al., 2010; Čopič et al., 2018; Gao et al., 2017). However, we cannot

exclude the possibility that an additional lipase(s) may regulate LD homeostasis in *Drosophila* photoreceptor neurons.

Earlier studies in yeast, rat dopaminergic neurons, and human induced pluripotent stem cells have proposed that αSyn expression induces lipid dysregulation and LD accumulation, but the underlying mechanisms were unclear (Fanning et al., 2019; Outeiro and Lindquist, 2003; Sánchez Campos et al., 2018). Low levels of αSyn accumulation were thought to perturb lipid homeostasis by enhancing unsaturated FA synthesis and the subsequent accumulation of diacylglycerols (DGs) and TGs. In the present study, we showed that αSyn expression alone did not enhance the accumulation of LDs but instead required concomitant overexpression of PLINs. Moreover, αSyn^{WT} expression alone had no effect on DG, TG, or LD content in *Drosophila* photoreceptor neurons. Given that αSyn and PLINs co-localized at the LD surface in both *Drosophila* photoreceptor neurons and human neuroblastoma cells, our results suggest the possibility that LD-associated αSyn could have a direct role in promoting neutral lipid accumulation by stabilizing LDs. Age-related accumulation of PLIN-bound LDs has been observed in fly muscles (Yan et al., 2017); however, further analyses will be required to determine whether this occurs in neurons and/or whether it is enhanced by αSyn.

The role of LDs in the evolution of PD pathology is the subject of intense scrutiny. LDs have been proposed to protect cells from lipotoxicity. Selkoe and colleagues showed that LD accumulation in yeast cells required TG synthesis, protected against elevated levels of oleic acid or DGs, and prevented αSyn toxicity (Fanning et al., 2019). The results of the present study suggest an alternative but not mutually exclusive role for LDs in promoting αSyn misfolding and conversion to a proteinase K-resistant form. Indeed, increased LD surface could provide a physical platform for αSyn deposition and conversion. For example, in a *Drosophila* model of PD induced by glucosylcerebrosidase-β deficiency, binding to glucosylceramide increased αSyn resistance to proteinase K (Suzuki et al., 2015). Based on a combination of our results and these observations, we propose a model of LD homeostasis in healthy and diseased neurons (Figure 6). In healthy neurons, relatively few LDs are detected due to a combination of low basal rate of TG synthesis and low expression of peridroplet proteins that promote LD stabilization. In pathological conditions such as PD, possibly in combination with age-dependent accumulation of fat and PLINs (Conte et al.,

2019; Yan et al., 2017), αSyn and PLINs could cooperate to promote the stabilization and accumulation of LDs in neurons. In this case, a pathogenic feed-forward mechanism is created in which αSyn enhances PLIN-dependent LD stabilization, which, in turn, increases αSyn conversion to a proteinase K-resistant form, culminating in αSyn aggregation and formation of cytoplasmic inclusion bodies. Collectively, our results raise the possibility that αSyn binding to LDs could be an important step in the pathogenesis of PD.

Material and Methods

Fly Stocks

All flies used for this study were raised on regular yeast medium at 25°C on a 12h light/dark cycle. The fly stocks were obtained as follows. *UAS-αSyn*^{WT} (BL8146), *UAS-αSyn*^{A53T} (BL8148), *UAS-Mdy-RNAi* (BL65963), *UAS-Bmm-RNAi* (BL25926), *UAS-GFP-shRNA* (BL41555), *sGMR-GAL4*, *Rh1-GAL4* (BL8688), *TH-GAL4* (Alex Whitworth/Léo Pallanck), *UAS-CG7900* (EY10020, BL17633), *UAS-LacZ* (BL1777) were from Bloomington *Drosophila* Stock Center. *UAS-dFatp-RNAi* (100124), *UAS-LacZ-RNAi* (51446) and *UAS-CG7900-RNAi* (101025) were from Vienna *Drosophila* Resource Center. *UAS-dPlin1::GFP* (Beller et al., 2010), *UAS-dPlin2::GFP* (Grönke et al., 2003) (second and third chromosome insertions), and *UAS-Bmm* were kindly provided by R.P. Kuhnlein (University of Graz); *UAS-LD*^{BD}*-GFP* was provided by M. Welte (Yu et al., 2011); and *UAS-αSyn*^{WT} (second chromosome insertion) was provided by M.B. Feany.

Cell Culture

The human neuroblastoma cell line SH-SY5Y was obtained from T. Baron (ANSES, Lyon, France) and transfected with 1 µg of a pcDNA3.1 vector containing human αSyn^{WT} cDNA (provided by T. Baron, Anses, Lyon, France) using Effecten transfection reagent (Qiagen). Positive clones were selected using geneticin and cultured in Dulbecco's modified Eagle's medium (DMEM/F-12, Gibco) supplemented with 4.5 g/L D-glucose, 10% fetal bovine serum, 100 U/mL penicillin, and 100 g/mL streptomycin at 37°C. Cells were passaged when they reached 70–80% confluence.

Bodipy Staining

Unless otherwise stated, experiments were performed using 20-day-old female flies. Flies were sedated on ice, decapitated, and the retinas were dissected in a drop of HL3 medium (Stewart et al., 1994). Whole-mount retinas were fixed in 4% paraformaldehyde (PFA), briefly washed in PBS supplemented with 0.1% Triton X-100 (PBS-T), and incubated overnight at 4°C in Bodipy 493/503 (D3922, Molecular Probes) diluted in PBS-T supplemented with 1:400 phalloidin-rhodamine (R415, Molecular Probes). The retinas were rinsed once in PBS-T and then mounted on a bridged slide in Vectashield medium. Samples

were examined on a Zeiss LSM800 at the LYMIC-PLATIM – Imaging and Microscopy Core Facility of SFR Biosciences (UMS3444), Lyon, France.

Bodipy Quantification

Retina images were acquired on a Zeiss LSM800 confocal microscope as 16-bit stacks and processed for quantification using ImageJ software (Schneider et al., 2012). Images were first filtered for noise using Gaussian Blur 3D ($\sigma = 1$) and projected along the Z-axis. LDs were identified using the Otsu thresholding algorithm. The area of Bodipy staining was measured and divided by the total retinal area as previously described (Van Den Brink et al., 2018).

Immunohistochemistry

Flies were sedated on ice, decapitated, and retinas were dissected in a drop of HL3 medium (Stewart et al., 1994) supplemented with D-glucose (120 mM). Whole-mount retinas were fixed in 4% PFA and permeabilized in PBS supplemented with 0.5% Triton X-100 and 5 mg/mL BSA. Mouse anti-Na+/K+ ATPase α-subunit (a5, DSHB), rabbit anti-GFP (A6455, Invitrogen), mouse anti-αSyn (sc-12767, Santa Cruz Biotechnology), or rabbit anti-dPlin2 (Grönke et al., 2003) a gift from R.P. Kuhnlein) primary antibodies were diluted in blocking solution and incubated with the retinas overnight at 4°C. The samples were then washed and incubated overnight at 4°C in blocking solution containing Alexa Fluor-conjugated anti-mouse Alexa488, anti-rabbit Alexa488, or anti-mouse Alexa647 secondary antibodies together with phalloidin-rhodamine to label F-actin.

SH-SY5Y cells were fixed with 4% PFA for 15 min and permeabilized with PBS containing 5% BSA and 0.05% saponin for 15 min. Cells were then incubated with mouse anti-αSyn (1:2000, sc-12767, Santa Cruz Biotechnology) and rabbit anti-PLIN3 (1:500, NB110, Novus Biologicals) primary antibodies at room temperature for 1 h. The cells were then washed and incubated with Bodipy 493/503 (D3922, Molecular Probes) and Alexa Fluor-conjugated anti-rabbit Alexa488/Alexa546 or anti-mouse Alexa647 secondary antibodies. Nuclei were counterstained with 1 µg/mL DAPI. Slides were mounted in Mowiol 4-88 (Sigma-Aldrich) and imaged with a Zeiss LSM800 confocal microscope.

Proximity Ligation Assay (PLA)

PLAs were performed using Duolink® PLA kits (Sigma) according to the manufacturer's instructions. Briefly, cells were fixed in 4% PFA and incubated with mouse anti-αSyn (1:2000, sc-12767, Santa Cruz Biotechnology) and rabbit anti-PLIN3 (1:500, NB110, Novus Biologicals) antibodies diluted in PBS containing 5% BSA and 0.05% saponin. The cells were then incubated with Duolink probes (anti-rabbit plus, DIO88002 and anti-mouse minus DIO82004).The PLA signal was revealed using the red Duolink In Situ Detection Reagent (DUO92008) and the cells were stained with Bodipy 493/503 (D3922, Molecular Probes). Nuclei were counterstained with DAPI in Mowiol mounting medium.

Mapping of *UAS-αSyn^{A53T}* Insertion Site

UAS-αSyn^{A53T} genomic localization was mapped using the Splinkerette protocol for mapping of transposable elements in *Drosophila* (Potter and Luo, 2010). Briefly, genomic DNA was isolated from one fly (stock BL8148) and digested using BstYI. DNA fragments containing the P-element flanking regions were then amplified using primers specific for pCaSpeR based P-element. The resulting DNA fragments were sequenced and mapped to the *Drosophila* genome using the BLAST platform.

Transmission Electron Microscopy (TEM) of *Drosophila* Eyes

TEM sample preparation was performed as previously described (Van Den Brink et al., 2018). Briefly, *Drosophila* eyes were fixed in 0.1 M cacodylate buffer supplemented with 2.5% glutaraldehyde and 2 mM $CaCl_2$ for 16 h at 4°C. After rinsing with 0.1 M cacodylate, the tissues were contrasted by incubation in 1% OsO_4 in 0.1 M cacodylate buffer for 2 h at room temperature. Tissues were then dehydrated in acetone and mounted in 100% epoxy resin (Epon 812). After resin polymerization, samples were sliced into 60 nm sections, stained with lead citrate, and examined with a Philips CM120 TEM operating at 80 kV.

Lipid Extraction and Quantification by Shotgun Mass Spectrometry

Ten retinas per biological sample were homogenized twice for 5 min each with 1 mm zirconia beads in 300 µl isopropanol using a cooled Tissuelyzer II at 30 Hz. The homogenate was evaporated in a vacuum desiccator to complete dryness, and lipids were extracted as

described (Knittelfelder et al., 2020; Sales et al., 2017). After evaporation, the samples were reconstituted in 300 µL 1:2 $CHCl_3$:MeOH. To quantify sterols, 200 µL aliquots of lipid extracts were evaporated and acetylated with 300 µL 2:1 $CHCl_3$:acetyl chloride for 1 h at room temperature (method modified from (Liebisch et al., 2006)). After evaporation, sterol samples were reconstituted in 200 µL 4:2:1 isopropanol:MeOH:$CHCl_3$ with 7.5 mM ammonium formate (spray solution). For sterol and lipidome measurements, samples were diluted 1:1 with spray solution. Mass spectrometric analysis was performed as described (Knittelfelder et al., 2020).

RNA Extraction and qRT-PCR

Total RNA was extracted from three sets of 10 *Drosophila* heads using TRI-Reagent (T9424, Sigma) and RNA was reverse transcribed using an iScript cDNA Synthesis Kit (Bio-Rad) according to the manufacturers' instructions. Quantitative PCR reactions were carried out using FastStart Universal SYBER Green Master mix (Roche Applied Science) on a StepOnePlus system (Applied Biosystems). Primer efficiency (E) was assessed using serial dilutions of cDNA preparations. Standard curves were used to determine the relationship between PCR cycle number (Ct) and mRNA abundance. Relative mRNA quantity (Qr) was calculated as: Qr = $E^{Ct_{Rp49}-Ct_{target}}$. Qr values were then normalized to control genotype. Experiments were performed using the following primers: *CG7900*: 5′-CTGCTCACTCTCAGCGTTCAG-3′ and 5′-ATATGTGCGAACCAACTCCAC-3′; *Rp49*: 5′-ATCGTGAAGAAGCGCACCAAG-3′ and 5′-ACCAGGAACTTCTTGAATCCG-3′.

Proteinase K-Resistance Assay

Fly heads were homogenized in lysis buffer (50 mM Tris-HCl pH 7.5, 5 mM EDTA, 0.1% NP40, 1 mM DTT, and 1% Protease Inhibitor Cocktail), incubated for 1 h at 25°C, and centrifuged at 13,000 rpm for 1 min. Supernatants were collected and incubated for 30 min at 25°C with proteinase K (0, 0.5, 1, 1.5, or 2 µg/mL). Denaturing buffer TD4215 4X was added to each sample, and proteins were separated in 4%–15% gradient acrylamide gels (Bio-Rad) and transferred to PVDF membranes (Millipore). PVDF membranes were fixed in 4% PFA and 0.01% glutaraldehyde in PBS for 30 min and then blocked in 3% BSA/0.1% Tween/PBS for XX h. Membranes were incubated with rabbit anti-α-Syn (MJFR1, ab138501, Abcam; 1:1000) or

mouse anti-β-tubulin (T 6199, Sigma, 1:1000) primary antibodies overnight at 4°C, washed, and incubated with horseradish peroxidase-conjugated anti-mouse IgG or anti-rabbit IgG (both from Pierce, 1:1000). After washing, membranes were incubated with SuperSignal West Dura Chemiluminescence Substrate (Thermo Scientific), and images were acquired using a ChemiDoc MP system (Bio-Rad).

Statistical Analysis

Data are presented as the means ± standard deviation (SD) of three experiments unless noted. Statistical analyses were performed using R software. Differences between groups were analyzed by t-test or ANOVA and Tukey's HSD paired sample comparison test depending on the number of groups, as specified in the figure legends.

Acknowledgements

We thank the ARTHRO-TOOLS and PLATIM microscopy platforms of SFR Biosciences (UMS3444/CNRS, US8/INSERM, ENS de Lyon, UCBL) and the Centre Technologique des Microstructures CTμ at Lyon 1 University. This work was supported by a grant from ENS Fond Recherche to BM. VG was supported by the Laboratory of Modelling and Biology of the Cell, Servier Research Institute, a PhD fellowship from Fondation pour la Recherche Medicale, and salary support from ENS Fond Recherche. Work in the Shevchenko laboratory was supported by Deutsche Forschungsgemeinschaft (grant FOR 2682).

Conflicts of Interest

The authors declare that they have no competing interests.

Figure Legends

Figure 1. αSyn enhances dPlin2-induced LD accumulation in *Drosophila* photoreceptor neurons.

(A) Longitudinal optical sections of whole-mount retinas from flies expressing *GFP* (control), *dPlin1::GFP*, or *dPlin2::GFP* in photoreceptor neurons (*Rh1-GAL4*). LDs are labeled green (lipophilic dye Bodipy D3922) and photoreceptor rhabdomeres are in magenta (phalloidin-rhodamine labeling of F-actin). Scale bar, 10 µm.

(B) Quantification of LD area expressed as % of total retinal area. Data are from the images shown in (A). Mean ± SD. ***p<0.001 by ANOVA with Tukey's HSD test.

(C) Longitudinal optical sections of whole-mount retinas from flies expressing *dPlin1::GFP* or *dPlin2::GFP* in photoreceptor neurons (*Rh1-GAL4*). Photoreceptor plasma membranes are in cyan (anti-Na^+/K^+ ATPase immunostaining) and rhabdomeres are in magenta(phalloidin-rhodamine labeling of F-actin). dPlin1 and dPlin2 are visible as ring shapes in the photoreceptor cytoplasm (yellow arrowheads). Scale bar, 10 µm.

(D) Longitudinal optical sections of whole-mount retinas from flies expressing LacZ (control) or human αSyn^{WT} alone or in conjunction with *dPlin2::GFP* in photoreceptor neurons (*Rh1-GAL4*). LDs are in green (Bodipy) and photoreceptor rhabdomeres are in magenta phalloidin-rhodamine labeling of F-actin). Scale bar, 10 µm.

(E) Quantification of LD area from the images shown in (D). Mean ± SD. ***p<0.001, ** p<0.05 by ANOVA with Tukey's HSD test.

Figure 2. αSyn co-localizes with PLINs at the surface of LDs in *Drosophila* photoreceptor neurons and human neuroblastoma cells.

(A) Longitudinal optical sections of whole-mount retinas from flies expressing αSyn^{WT} and *dPlin2::GFP* in photoreceptor neurons (*Rh1-GAL4*). αSyn is in magenta (immunostaining) and photoreceptor rhabdomeres are in red (phalloidin-rhodamine labeling of F-actin). White arrowheads indicate co-localization of αSyn and dPlin2 at LDs. Scale bar, 5 µm.

(B) High-resolution Airyscan micrograph of SH-SY5Y neuroblastoma cells transfected with αSyn^{WT}. αSyn and endogenous PLIN3 immunostaining are shown in magenta and green, respectively. Nuclei are counterstained with DAPI (cyan). Arrowheads indicate co-localization of αSyn and PLIN3 staining on LDs. Scale bar, 5 µm.

(C) Proximity ligation assay between αSyn and PLIN3 in SH-SY5Y cells transfected with human αSyn^{WT}. The PLA signal generated by close proximity of the two protein-bound primary antibodies is shown in magenta, LDs are in green (Bodipy), and nuclei are counterstained with DAPI (cyan). Scale bars, 5 µm.

Figure 3. LD abundance in photoreceptor neurons is not affected by knockdown of enzymes involved in TG synthesis (*Fatp*, *Mdy*) or degradation (*Bmm*).

(A) Longitudinal optical sections of whole-mount retinas from flies expressing RNAi targeting *Bmm* lipase under the control of the pan-retinal driver *GMR-GAL4* or the photoreceptor-specific driver *Rh1-GAL4*. LDs are visible in green (Bodipy) and photoreceptor rhabdomeres are in magenta (phalloidin-rhodamine labeling of F-actin). Pan-retinal *Bmm* knockdown leads to LD accumulation in retinal glial cells between photoreceptor cells (left panel), but LDs are not detected in flies with photoreceptor neuron-specific Bmm knockdown (right panel). Scale bar, 10 µm.

(B) Longitudinal optical sections of whole-mount retinas from flies with pan-retinal knockdown of *Bmm* lipase. dPlin2 is shown in green (immunostaining), photoreceptor plasma membrane is in cyan (Na^+/K^+ ATPase immunostaining), and photoreceptor rhabdomeres are in magenta (phalloidin-rhodamine labeling of F-actin). White arrowheads indicate LDs in glial cells, juxtaposed between the plasma membrane and rhabdomeres. Scale bar, 10 µm.

(C) Longitudinal optical sections of whole-mount retina from flies with photoreceptor neuron-specific expression of *dPlin1::GFP* and *LacZ-RNAi* (control), *dFatp-RNAi,* or *Mdy-RNAi*. LDs are in green (Bodipy) and photoreceptor rhabdomeres are in magenta (phalloidin-rhodamine labeling of F-actin). Scale bar, 10 µm.

(D) Quantification of LD area from the images shown in (C). Mean ± SD. ns, not significant, *$p<0.05$, by ANOVA with Tukey's HSD test.

(E) Longitudinal optical sections of whole-mount retina from flies with photoreceptor neuron-specific expression of *LacZ* (control), Klarsicht lipid-binding domain (LD^{BD}-GFP), or the *FAAH2* ortholog *CG7900*. LDs are shown in green (Bodipy) and photoreceptor rhabdomeres in magenta (phalloidin-rhodamine labeling of F-actin). Scale bar, 10 µm.

(F) Quantification of LD area from the images shown in (E). Mean ± SD. ***p<0.001 by ANOVA with Tukey's HSD test.

Figure 4. Characterization of the *P{UAS-αSyn^{A53T}}CG7900* transgenic line promoting LD accumulation in photoreceptors

(A) Schematic illustration of the genomic localization of the *P{UAS-αSyn^{A53T}}* transgene mapped using the Splinkerette protocol. The P element carrying the yeast minimal promoter UAS upstream of the coding sequence of human *αSyn^{A53T}* is inserted in the promoter region of *CG7900*.

(B) qRT-PCR analysis of *CG7900* mRNA in whole flies expressing *LacZ, αSyn^{A53T}-CG7900,* or *CG7900* (EP-[UAS] insertion, EY10020) under the control of the pan-retinal driver *GMR-GAL4*. mRNA levels are expressed as the mean ± SD of triplicates relative to the level in control (*GMR>LacZ*) flies.

(C) Longitudinal optical sections of whole-mount retinas from flies with pan-retinal expression of *GFP* or *αSyn^{A53T}-CG7900*. LDs are shown in green (Bodipy) and photoreceptor rhabdomeres are in magenta (phalloidin-rhodamine labeling of F-actin). Scale bar, 20 µm.

(D) TEM images of ommatidia cross-sections from 60-day-old flies with pan-retinal expression of *GFP* (top panel) or *αSyn^{A53T}-CG7900* (bottom panel). Each panel shows a representative cross-section of one ommatidium containing seven photoreceptors (false-colored blue) with central rhabdomeres (R) surrounded by retinal glial cells (false-colored orange). Yellow asterisks indicate LDs accumulating in the photoreceptor cytoplasm of flies expressing *αSyn^{A53T}-CG7900*. Scale bar, 2 µm.

(E) Longitudinal optical sections of whole-mount retinas from flies expressing *αSyn^{A53T}-CG7900* alone or in conjunction with Bmm in photoreceptors (*Rh1-GAL4*). LDs are shown in green (Bodipy) and photoreceptor rhabdomeres are in magenta (phalloidin-rhodamine labeling of F-actin). Scale bar, 20 µm.

(F). Quantification of LD area from the images shown in (E). Mean ± SD. ***p<0.001 by t-test.

Figure 5. LD depletion by expression of *Bmm* lipase reduces αSyn resistance to proteinase K.

(A) αSyn proteinase K-resistance assay. Lysates of the heads of 6- and 30-day-old flies with photoreceptor neuron-specific expression of *αSyn^{A53T}-CG7900* and either *LacZ* (control) or *Bmm* lipase were digested with the indicated concentrations of proteinase K and then immunoblotted for αSyn or β-tubulin (loading control).

(B) Quantification of proteinase K-resistant αSyn, as analyzed in (A). Resistance is expressed as the ratio of undigested αSyn remaining after treatment with 2 µg/mL of proteinase K relative to the untreated sample.

Figure 6. Model of the contribution of αSyn to LD accumulation in PD.

Under normal physiological conditions, neurons contain relatively few LDs. We propose the following scenario under pathological conditions associated with elevated levels of αSyn and dPlin2: **(1)** LDs are stabilized by the increase dPlin2; **(2)** αSyn binds to the expanding dPlin2-positive LDs, which further increases LD accumulation; **(3)** αSyn is converted to a proteinase K-resistant form(s) on the surface of LDs; and **(4)** the aberrant form of αSyn may aggregate at the surface of or in close proximity to LDs, leading to formation of cytoplasmic inclusion bodies (Dettmer et al., 2017).

Bibliography

Auluck, P.K., Chan, H.Y.E., Trojanowski, J.Q., Lee, V.M.-Y., and Bonini, N.M. (2002). Chaperone Suppression of a-Synuclein Toxicity in a Drosophila Model for Parkinson's Disease. Science *295*, 862–865.

Auluck, P.K., Caraveo, G., and Lindquist, S. (2010). α-Synuclein: membrane interactions and toxicity in Parkinson's disease. Annu. Rev. Cell Dev. Biol. *26*, 211–233.

Bailey, A.P., Koster, G., Guillermier, C., Hirst, E.M.A., MacRae, J.I., Lechene, C.P., Postle, A.D., and Gould, A.P. (2015). Antioxidant Role for Lipid Droplets in a Stem Cell Niche of Drosophila. Cell *163*, 340–353.

Beller, M., Bulankina, A.V., Hsiao, H.-H., Urlaub, H., Jäckle, H., and Kühnlein, R.P. (2010). PERILIPIN-Dependent Control of Lipid Droplet Structure and Fat Storage in Drosophila. Cell Metab. *12*, 521–532.

Beller, M., Herker, E., and Füllekrug, J. (2020). Grease on—Perspectives in lipid droplet biology. Semin. Cell Dev. Biol.

Bersuker, K., and Olzmann, J.A. (2017). Establishing the lipid droplet proteome: Mechanisms of lipid droplet protein targeting and degradation. Biochim. Biophys. Acta BBA - Mol. Cell Biol. Lipids *1862*, 1166–1177.

Bersuker, K., Peterson, C.W.H., To, M., Sahl, S.J., Savikhin, V., Grossman, E.A., Nomura, D.K., and Olzmann, J.A. (2018). A Proximity Labeling Strategy Provides Insights into the Composition and Dynamics of Lipid Droplet Proteomes. Dev. Cell *44*, 97-112.e7.

Bi, J., Xiang, Y., Chen, H., Liu, Z., Grönke, S., Kühnlein, R.P., and Huang, X. (2012). Opposite and redundant roles of the two Drosophila perilipins in lipid mobilization. J. Cell Sci. *125*, 3568–3577.

Brasaemle, D.L. (2007). Thematic review series: adipocyte biology. The perilipin family of structural lipid droplet proteins: stabilization of lipid droplets and control of lipolysis. J. Lipid Res. *48*, 2547–2559.

Bussell, R., and Eliezer, D. (2003). A Structural and Functional Role for 11-mer Repeats in α-Synuclein and Other Exchangeable Lipid Binding Proteins. J. Mol. Biol. *329*, 763–778.

Buszczak, M., Lu, X., Segraves, W.A., Chang, T.Y., and Cooley, L. (2002). Mutations in the midway gene disrupt a Drosophila acyl coenzyme A: diacylglycerol acyltransferase. Genetics *160*, 1511–1518.

Chouhan, A.K., Guo, C., Hsieh, Y.-C., Ye, H., Senturk, M., Zuo, Z., Li, Y., Chatterjee, S., Botas, J., Jackson, G.R., et al. (2016). Uncoupling neuronal death and dysfunction in Drosophila models of neurodegenerative disease. Acta Neuropathol. Commun. *4*.

Cole, N.B., Murphy, D.D., Grider, T., Rueter, S., Brasaemle, D., and Nussbaum, R.L. (2002). Lipid droplet binding and oligomerization properties of the Parkinson's disease protein alpha-synuclein. J. Biol. Chem. *277*, 6344–6352.

Conte, M., Martucci, M., Sandri, M., Franceschi, C., and Salvioli, S. (2019). The Dual Role of the Pervasive "Fattish" Tissue Remodeling With Age. Front. Endocrinol. *10*, 114.

Cooper, A.A., Gitler, A.D., Cashikar, A., Haynes, C.M., Hill, K.J., Bhullar, B., Liu, K., Xu, K., Strathearn, K.E., Liu, F., et al. (2006). α-Synuclein Blocks ER-Golgi Traffic and Rab1 Rescues Neuron Loss in Parkinson's Models. Science *313*, 324–328.

Čopič, A., Antoine-Bally, S., Giménez-Andrés, M., La Torre Garay, C., Antonny, B., Manni, M.M., Pagnotta, S., Guihot, J., and Jackson, C.L. (2018). A giant amphipathic helix from a perilipin that is adapted for coating lipid droplets. Nat. Commun. *9*.

Cremades, N., Cohen, S.I.A., Deas, E., Abramov, A.Y., Chen, A.Y., Orte, A., Sandal, M., Clarke, R.W., Dunne, P., Aprile, F.A., et al. (2012). Direct Observation of the Interconversion of Normal and Toxic Forms of α-Synuclein. Cell *149*, 1048–1059.

Dettmer, U., Ramalingam, N., von Saucken, V.E., Kim, T.-E., Newman, A.J., Terry-Kantor,

E., Nuber, S., Ericsson, M., Fanning, S., Bartels, T., et al. (2017). Loss of native α-synuclein multimerization by strategically mutating its amphipathic helix causes abnormal vesicle interactions in neuronal cells. Hum. Mol. Genet. *26*, 3466–3481.
Dourlen, P., Sujkowski, A., Wessells, R., and Mollereau, B. (2015). Fatty acid transport proteins in disease: New insights from invertebrate models. Prog. Lipid Res. *60*, 30–40.
Etschmaier, K., Becker, T., Eichmann, T.O., Schweinzer, C., Scholler, M., Tam-Amersdorfer, C., Poeckl, M., Schuligoi, R., Kober, A., Chirackal Manavalan, A.P., et al. (2011). Adipose triglyceride lipase affects triacylglycerol metabolism at brain barriers. J. Neurochem. *119*, 1016–1028.
Fanning, S., Haque, A., Imberdis, T., Baru, V., Barrasa, M.I., Nuber, S., Termine, D., Ramalingam, N., Ho, G.P.H., Noble, T., et al. (2019). Lipidomic Analysis of α-Synuclein Neurotoxicity Identifies Stearoyl CoA Desaturase as a Target for Parkinson Treatment. Mol. Cell *73*, 1001-1014.e8.
Fanning, S., Selkoe, D., and Dettmer, U. (2020). Parkinson's disease: proteinopathy or lipidopathy? NPJ Park. Dis. *6*, 3.
Farmer, B.C., Walsh, A.E., Kluemper, J.C., and Johnson, L.A. (2020). Lipid Droplets in Neurodegenerative Disorders. Front. Neurosci. *14*, 742.
Feany, M.B., and Bender, W.W. (2000). A Drosophila model of Parkinson's disease. Nature *404*, 394–398.
Galvagnion, C. (2017). The Role of Lipids Interacting with α-Synuclein in the Pathogenesis of Parkinson's Disease. J. Park. Dis. *7*, 433–450.
Gao, Q., Binns, D.D., Kinch, L.N., Grishin, N.V., Ortiz, N., Chen, X., and Goodman, J.M. (2017). Pet10p is a yeast perilipin that stabilizes lipid droplets and promotes their assembly. J. Cell Biol. *216*, 3199–3217.
Grönke, S., Beller, M., Fellert, S., Ramakrishnan, H., Jäckle, H., and Kühnlein, R.P. (2003). Control of fat storage by a Drosophila PAT domain protein. Curr. Biol. CB *13*, 603–606.
Grönke, S., Mildner, A., Fellert, S., Tennagels, N., Petry, S., Müller, G., Jäckle, H., and Kühnlein, R.P. (2005). Brummer lipase is an evolutionary conserved fat storage regulator in Drosophila. Cell Metab. *1*, 323–330.
Han, X., Zhu, J., Zhang, X., Song, Q., Ding, J., Lu, M., Sun, S., and Hu, G. (2018). Plin4-Dependent Lipid Droplets Hamper Neuronal Mitophagy in the MPTP/p-Induced Mouse Model of Parkinson's Disease. Front. Neurosci. *12*, 397.
Heier, C., and Kühnlein, R.P. (2018). Triacylglycerol Metabolism in Drosophila melanogaster. Genetics *210*, 1163–1184.
Ioannou, M.S., Jackson, J., Sheu, S.-H., Chang, C.-L., Weigel, A.V., Liu, H., Pasolli, H.A., Xu, C.S., Pang, S., Matthies, D., et al. (2019). Neuron-Astrocyte Metabolic Coupling Protects against Activity-Induced Fatty Acid Toxicity. Cell *177*, 1522-1535.e14.
Itabe, H., Yamaguchi, T., Nimura, S., and Sasabe, N. (2017). Perilipins: a diversity of intracellular lipid droplet proteins. Lipids Health Dis. *16*, 83.
Kaczocha, M., Glaser, S.T., Chae, J., Brown, D.A., and Deutsch, D.G. (2010). Lipid droplets are novel sites of N-acylethanolamine inactivation by fatty acid amide hydrolase-2. J. Biol. Chem. *285*, 2796–2806.
Kimmel, A.R., and Sztalryd, C. (2016). The Perilipins: Major Cytosolic Lipid Droplet-Associated Proteins and Their Roles in Cellular Lipid Storage, Mobilization, and Systemic Homeostasis. Annu. Rev. Nutr. *36*, 471–509.
Knittelfelder, O., Prince, E., Sales, S., Fritzsche, E., Wöhner, T., Brankatschk, M., and Shevchenko, A. (2020). Sterols as dietary markers for Drosophila melanogaster. Biochim. Biophys. Acta Mol. Cell Biol. Lipids *1865*, 158683.
Krahmer, N., Farese, R.V., and Walther, T.C. (2013). Balancing the fat: lipid droplets and human disease. EMBO Mol. Med. *5*, 973–983.

Lessing, D., and Bonini, N.M. (2009). Maintaining the brain: insight into human neurodegeneration from Drosophila melanogaster mutants. Nat. Rev. Genet. *10*, 359–370.
Liebisch, G., Binder, M., Schifferer, R., Langmann, T., Schulz, B., and Schmitz, G. (2006). High throughput quantification of cholesterol and cholesteryl ester by electrospray ionization tandem mass spectrometry (ESI-MS/MS). Biochim. Biophys. Acta *1761*, 121–128.
Liu, L., Zhang, K., Sandoval, H., Yamamoto, S., Jaiswal, M., Sanz, E., Li, Z., Hui, J., Graham, B.H., Quintana, A., et al. (2015). Glial Lipid Droplets and ROS Induced by Mitochondrial Defects Promote Neurodegeneration. Cell *160*, 177–190.
Liu, L., MacKenzie, K.R., Putluri, N., Maletić-Savatić, M., and Bellen, H.J. (2017). The Glia-Neuron Lactate Shuttle and Elevated ROS Promote Lipid Synthesis in Neurons and Lipid Droplet Accumulation in Glia via APOE/D. Cell Metab. *26*, 719-737.e6.
Mollereau, B., and Domingos, P.M. (2005). Photoreceptor differentiation in Drosophila: from immature neurons to functional photoreceptors. Dev. Dyn. Off. Publ. Am. Assoc. Anat. *232*, 585–592.
Olzmann, J.A., and Carvalho, P. (2019). Dynamics and functions of lipid droplets. Nat. Rev. Mol. Cell Biol. *20*, 137–155.
Ordonez, D.G., Lee, M.K., and Feany, M.B. (2018). α-synuclein Induces Mitochondrial Dysfunction through Spectrin and the Actin Cytoskeleton. Neuron *97*, 108-124.e6.
Outeiro, T.F., and Lindquist, S. (2003). Yeast cells provide insight into alpha-synuclein biology and pathobiology. Science *302*, 1772–1775.
Pennetta, G., and Welte, M.A. (2018). Emerging Links between Lipid Droplets and Motor Neuron Diseases. Dev. Cell *45*, 427–432.
Poewe, W., Seppi, K., Tanner, C.M., Halliday, G.M., Brundin, P., Volkmann, J., Schrag, A.-E., and Lang, A.E. (2017). Parkinson disease. Nat. Rev. Dis. Primer *3*, 17013.
Potter, C.J., and Luo, L. (2010). Splinkerette PCR for Mapping Transposable Elements in Drosophila. PLoS ONE *5*, e10168.
Ryu, E.J., Harding, H.P., Angelastro, J.M., Vitolo, O.V., Ron, D., and Greene, L.A. (2002). Endoplasmic reticulum stress and the unfolded protein response in cellular models of Parkinson's disease. J. Neurosci. Off. J. Soc. Neurosci. *22*, 10690–10698.
Sales, S., Knittelfelder, O., and Shevchenko, A. (2017). Lipidomics of Human Blood Plasma by High-Resolution Shotgun Mass Spectrometry. In Methods in Molecular Biology, pp. 203–212.
Sánchez Campos, S., Alza, N.P., and Salvador, G.A. (2018). Lipid metabolism alterations in the neuronal response to A53T α-synuclein and Fe-induced injury. Arch. Biochem. Biophys. *655*, 43–54.
Schneider, C.A., Rasband, W.S., and Eliceiri, K.W. (2012). NIH Image to ImageJ: 25 years of Image Analysis. Nat. Methods *9*, 671–675.
Schönfeld, P., and Reiser, G. (2013). Why does brain metabolism not favor burning of fatty acids to provide energy? Reflections on disadvantages of the use of free fatty acids as fuel for brain. J. Cereb. Blood Flow Metab. Off. J. Int. Soc. Cereb. Blood Flow Metab. *33*, 1493–1499.
Shahmoradian, S.H., Lewis, A.J., Genoud, C., Hench, J., Moors, T.E., Navarro, P.P., Castaño-Díez, D., Schweighauser, G., Graff-Meyer, A., Goldie, K.N., et al. (2019). Lewy pathology in Parkinson's disease consists of crowded organelles and lipid membranes. Nat. Neurosci. *22*, 1099–1109.
Sjöstedt, E., Zhong, W., Fagerberg, L., Karlsson, M., Mitsios, N., Adori, C., Oksvold, P., Edfors, F., Limiszewska, A., Hikmet, F., et al. (2020). An atlas of the protein-coding genes in the human, pig, and mouse brain. Science *367*.
Stewart, B.A., Atwood, H.L., Renger, J.J., Wang, J., and Wu, C.F. (1994). Improved stability of Drosophila larval neuromuscular preparations in haemolymph-like physiological solutions.

J. Comp. Physiol. [A] *175*, 179–191.
Suzuki, M., Fujikake, N., Takeuchi, T., Kohyama-Koganeya, A., Nakajima, K., Hirabayashi, Y., Wada, K., and Nagai, Y. (2015). Glucocerebrosidase deficiency accelerates the accumulation of proteinase K-resistant α-synuclein and aggravates neurodegeneration in a *Drosophila* model of Parkinson's disease. Hum. Mol. Genet. *24*, 6675–6686.
Suzuki, M., Sango, K., Wada, K., and Nagai, Y. (2018). Pathological role of lipid interaction with α-synuclein in Parkinson's disease. Neurochem. Int. *119*, 97–106.
Thiam, A.R., and Beller, M. (2017). The why, when and how of lipid droplet diversity. J. Cell Sci. *130*, 315–324.
Thiam, A.R., Antonny, B., Wang, J., Delacotte, J., Wilfling, F., Walther, T.C., Beck, R., Rothman, J.E., and Pincet, F. (2013). COPI buds 60-nm lipid droplets from reconstituted water–phospholipid–triacylglyceride interfaces, suggesting a tension clamp function. Proc. Natl. Acad. Sci. U. S. A. *110*, 13244–13249.
Van Den Brink, D.M., Cubizolle, A., Chatelain, G., Davoust, N., Girard, V., Johansen, S., Napoletano, F., Dourlen, P., Guillou, L., Angebault-Prouteau, C., et al. (2018). Physiological and pathological roles of FATP-mediated lipid droplets in Drosophila and mice retina. PLOS Genet. *14*, e1007627.
Walther, T.C., Chung, J., and Farese, R.V. (2017). Lipid Droplet Biogenesis. Annu. Rev. Cell Dev. Biol. *33*, 491–510.
Wang, S., Yoo, S., Kim, H.-Y., Wang, M., Zheng, C., Parkhouse, W., Krieger, C., and Harden, N. (2015). Detection of in situ protein-protein complexes at the Drosophila larval neuromuscular junction using proximity ligation assay. J. Vis. Exp. JoVE 52139.
Welte, M.A. (2015). Expanding Roles for Lipid Droplets. Curr. Biol. *25*, R470–R481.
Welte, M.A., and Gould, A.P. (2017). Lipid droplet functions beyond energy storage. Biochim. Biophys. Acta *1862*, 1260–1272.
Welte, M.A., Gross, S.P., Postner, M., Block, S.M., and Wieschaus, E.F. (1998). Developmental Regulation of Vesicle Transport in Drosophila Embryos: Forces and Kinetics. Cell *92*, 547–557.
Yan, Y., Wang, H., Hu, M., Jiang, L., Wang, Y., Liu, P., Liang, X., Liu, J., Li, C., Lindström-Battle, A., et al. (2017). HDAC6 Suppresses Age-Dependent Ectopic Fat Accumulation by Maintaining the Proteostasis of PLIN2 in Drosophila. Dev. Cell *43*, 99-111.e5.
Yasuhara, J.C., Baumann, O., and Takeyasu, K. (2000). Localization of Na/K-ATPase in developing and adult Drosophila melanogaster photoreceptors. Cell Tissue Res. *300*, 239–249.
Yu, Y.V., Li, Z., Rizzo, N.P., Einstein, J., and Welte, M.A. (2011). Targeting the motor regulator Klar to lipid droplets. BMC Cell Biol. *12*, 9.
Zechner, R., Zimmermann, R., Eichmann, T.O., Kohlwein, S.D., Haemmerle, G., Lass, A., and Madeo, F. (2012). FAT SIGNALS--lipases and lipolysis in lipid metabolism and signaling. Cell Metab. *15*, 279–291.

Girard et al. Figure 1

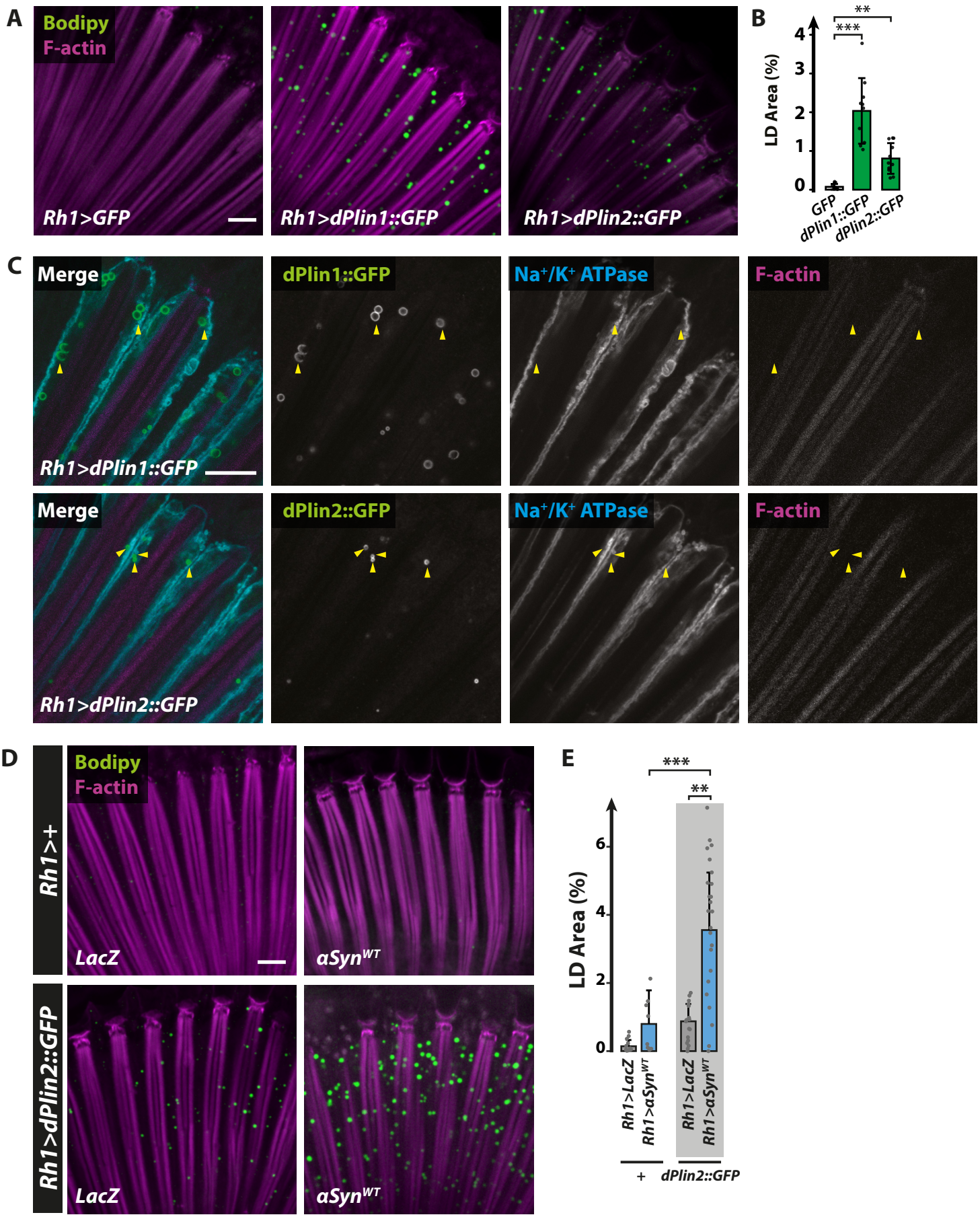

Girard et al. Figure 2

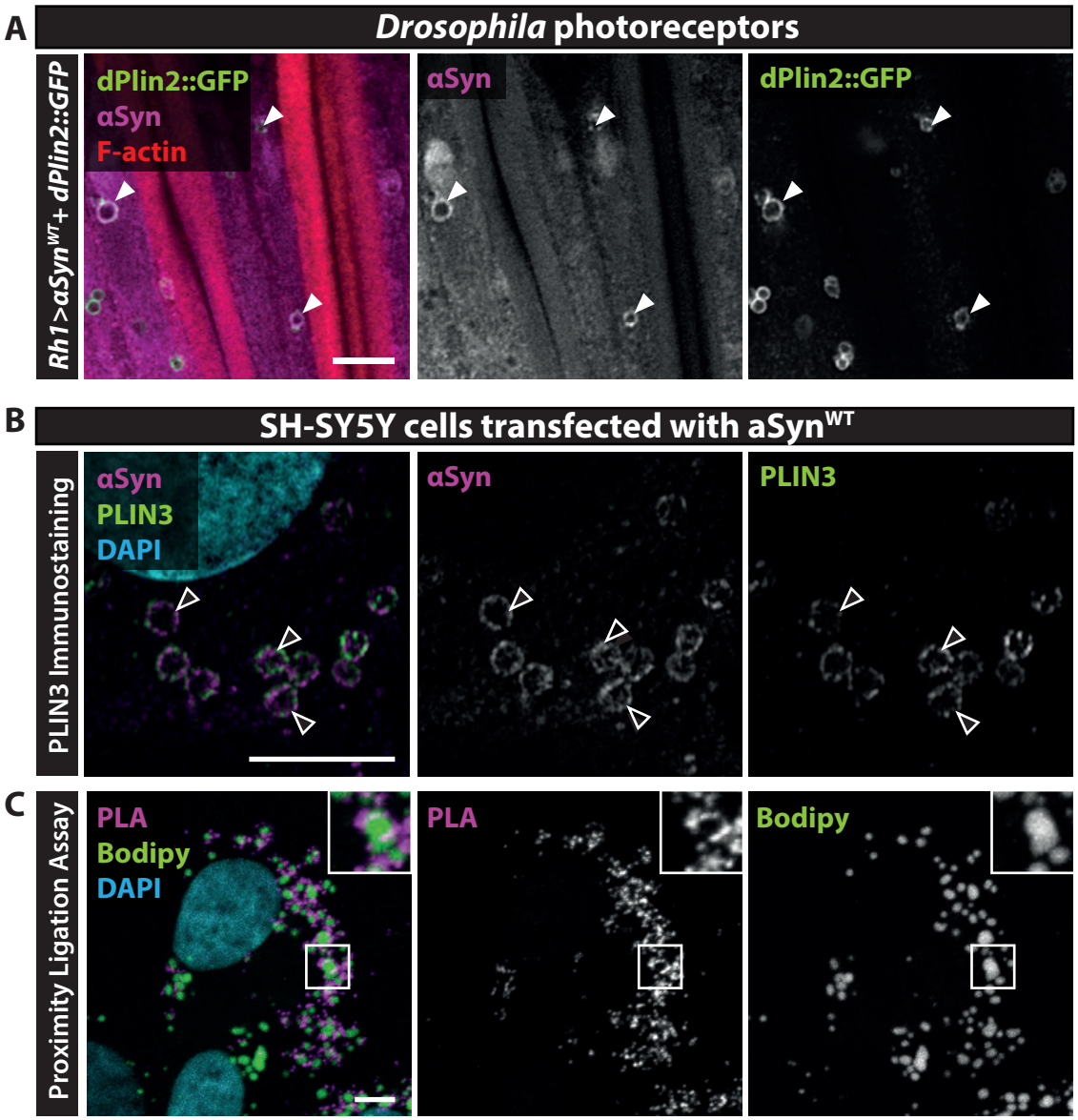

Girard et al. Figure 3

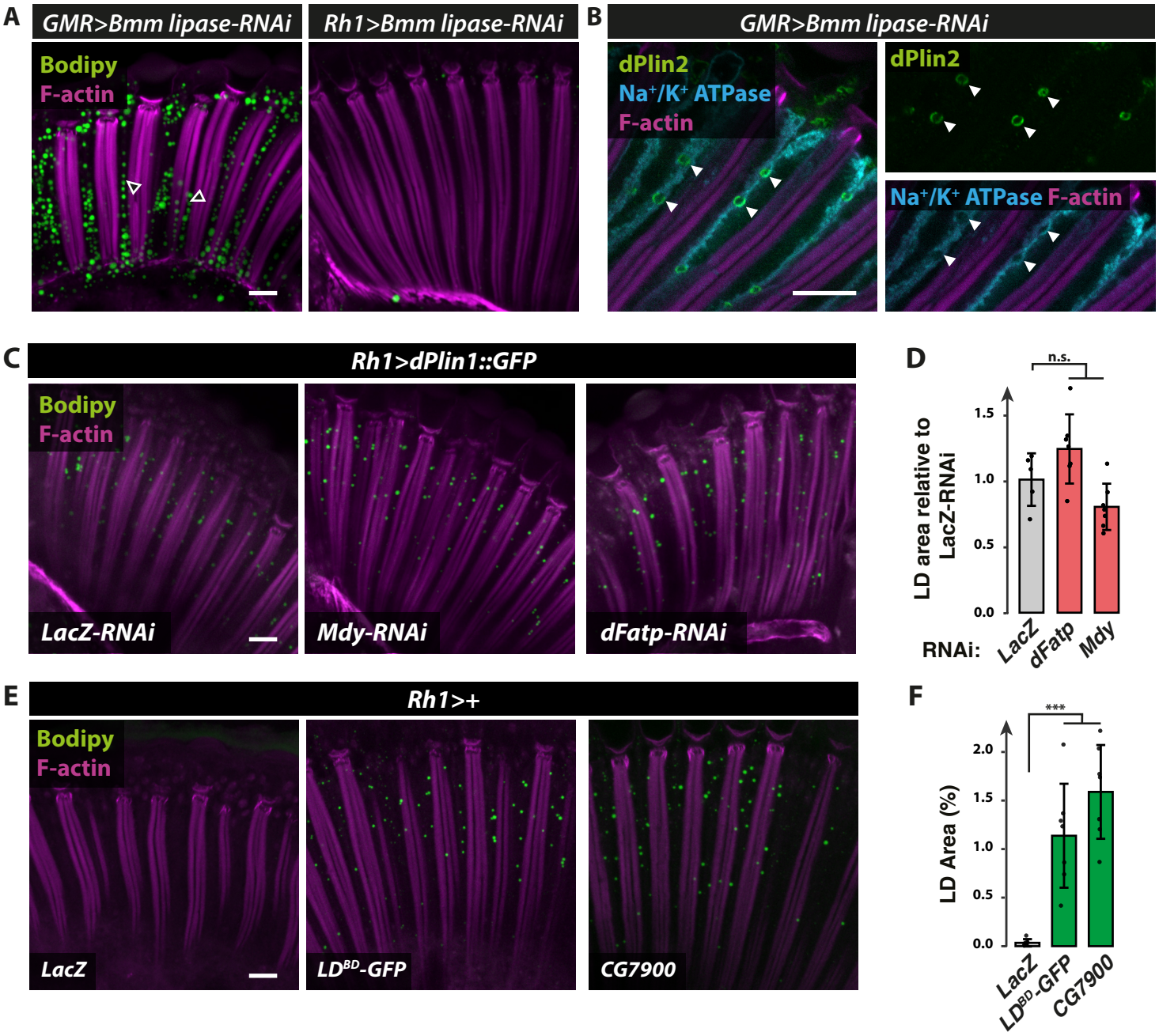

Girard et al. Figure 4

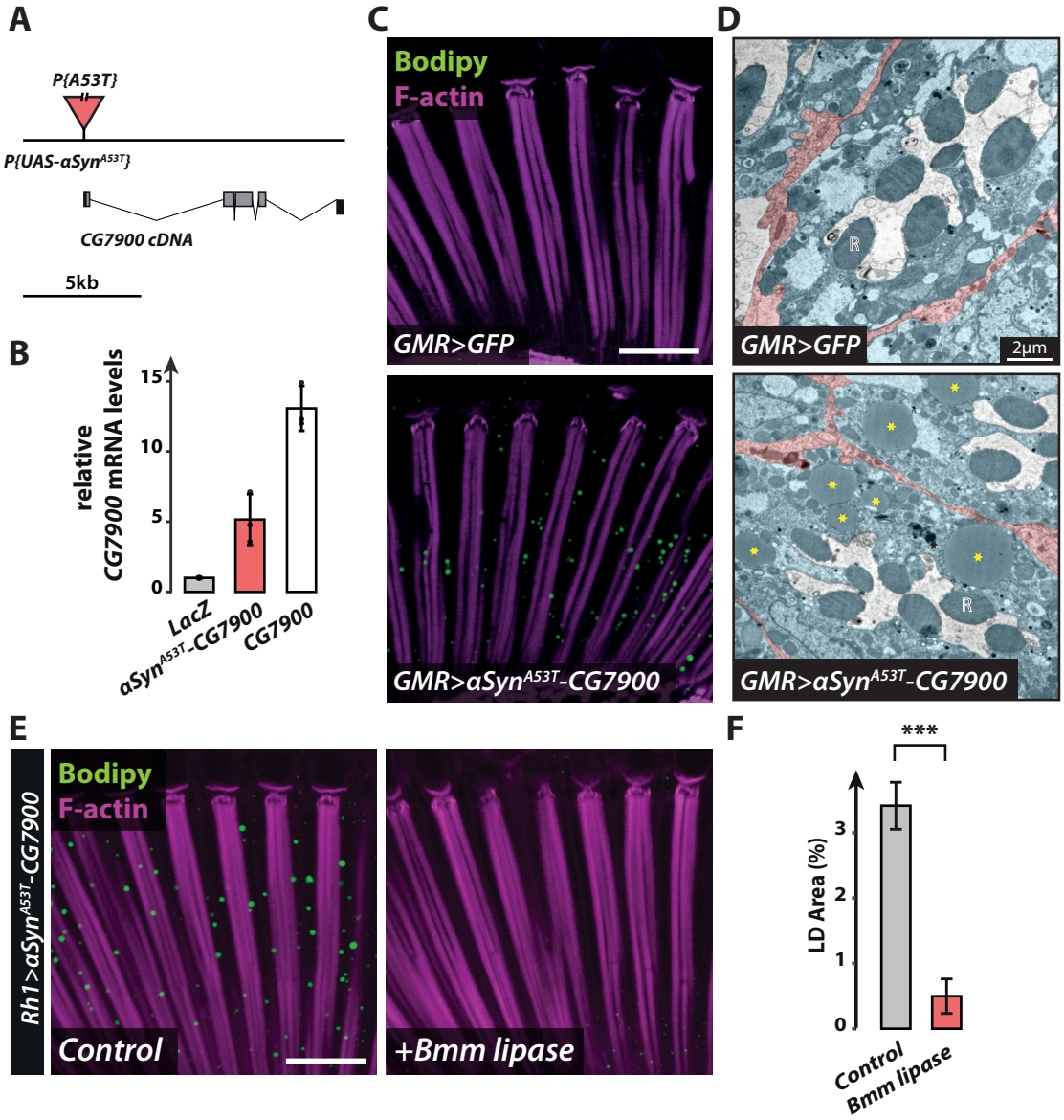

Girard et al. Figure 5

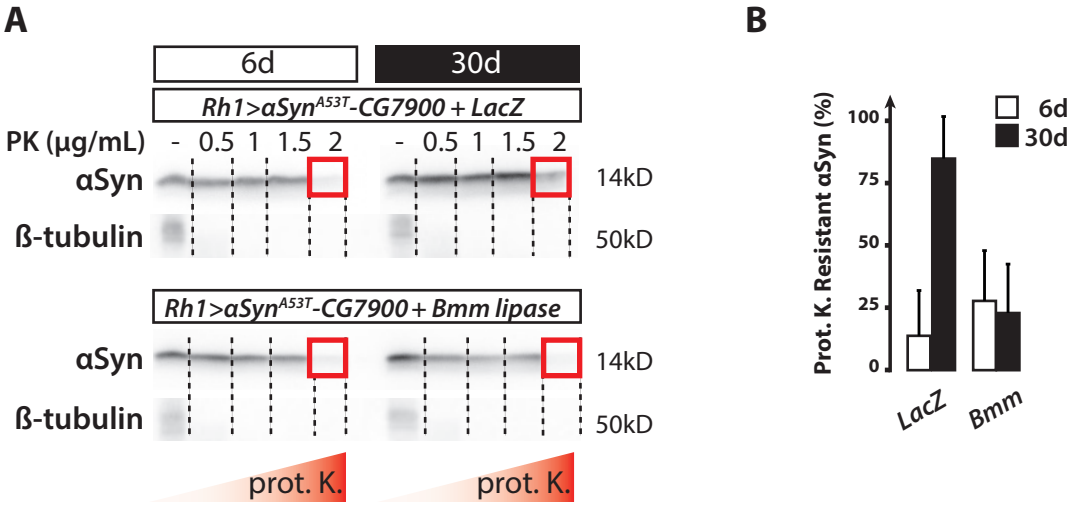
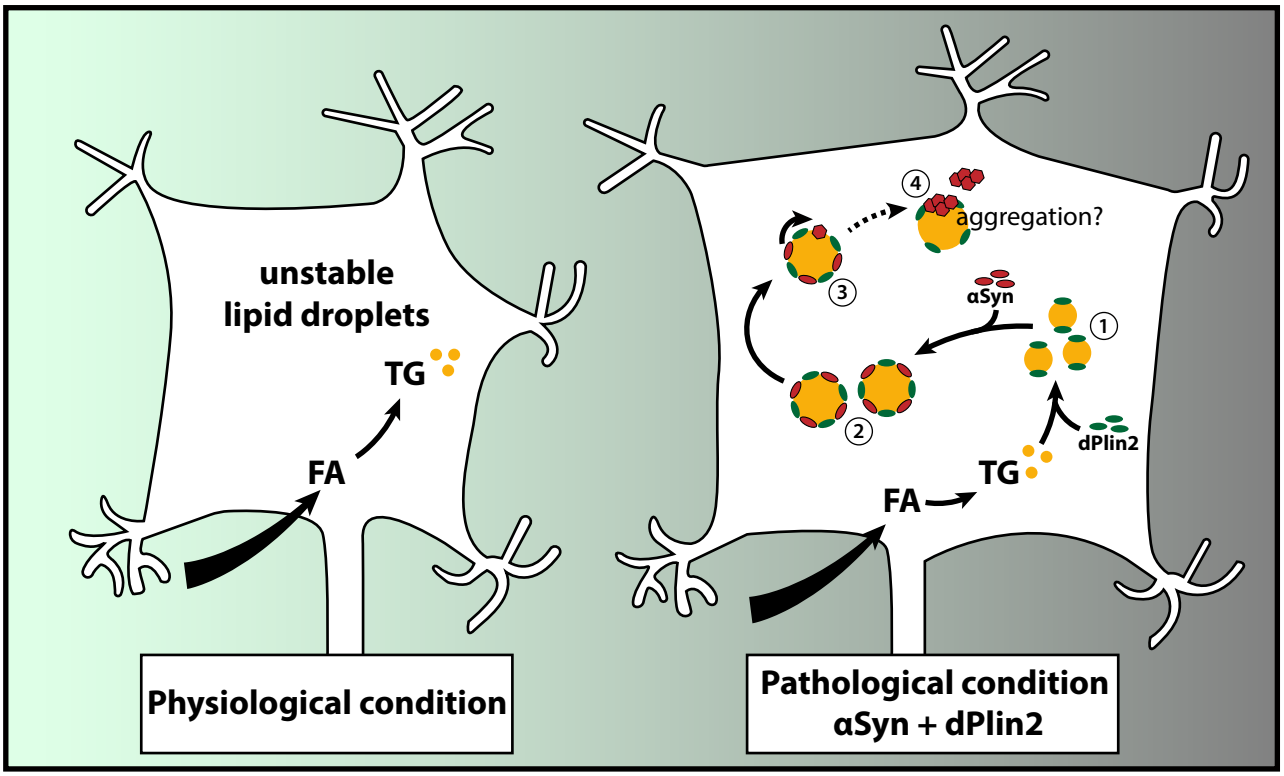
Girard et al. Figure 6